Computational Materials Science 159 (2019) 357–364

Contents lists available at ScienceDirect

Computational Materials Science

journal homepage: www.elsevier.com/locate/commatsci

A high-throughput computation framework for generalized stacking fault energies of pure metals

Peng Tu[a], Yonghao Zheng[a], Cheng Zhuang[a], Xiaoqin Zeng[b,*], Hong Zhu[a,*]

[a] University of Michigan – Shanghai Jiao Tong University Joint Institute, Shanghai Jiao Tong University, Shanghai 200240, PR China
[b] National Engineering Research Center of Light Alloys, School of Materials Science and Engineering, Shanghai Jiao Tong University, 200240 Shanghai, PR China

ARTICLE INFO

Keywords:
Workflow
First-principles calculations
Generalized stacking fault energy
Climbing image-nudged elastic band

ABSTRACT

Generalized stacking fault energy (GSFE) is an important property in understanding the plastic deformations of metals. However, the traditional way to calculate it one by one is not efficient, this work introduces a high-throughput workflow to calculate GSFEs using density functional theory (DFT) calculations and climbing image-nudged elastic band (CI-NEB) method. Based on open-source computational tools from the Materials Project infrastructure, this computation framework automates the procedure of building perfect and faulted slab models with certain orientations, performing DFT simulations and extracting the results into database. The computed GSFEs from this work and ductility parameter based on the GSFE are consistent with reported data from previous literatures, validating the accuracy of our results and algorithm. Such a GSFE workflow may speed up the development and understanding of the mechanical properties of metals or alloys by enabling the computations of GSFEs in an automatic and high-throughput way.

1. Introduction

The development of materials with better mechanical properties, i.e. high strength and high ductility, has been always important for traditional as well as high technology applications. Although the plastic deformation of materials is by nature a multiscale process, it is well accepted that dislocations play a direct or at least critical role [1]. Consequently, an accurate description of the long-range stress and strain fields produced by dislocations based on the elasticity theory of dislocations e.g. the Peierls-Nabaro (P-N) model [2,3] and the reasonable atomic-scale models of dislocation cores [4,5] are important to understand plastic deformations.

The dislocation core structures and mobility are partly controlled by the ease to shear a crystal along a given crystallographic plane, which can be characterized by the generalized stacking fault energies (GSFEs) or γ surfaces [5]. Thus, the determination of GSFEs appears to be an instructive first step towards the understanding of the plasticity of materials. The concept of GSFE or γ surface originally introduced by Vitek [6] represents the extra energy per unit area needed for sliding one half of the crystal relative to the other by a vector $\mathbf{v}$, which can be further used to denote the restoring force or the lattice resistance during dislocation nucleation, where $\mathbf{F}(\mathbf{v}) = -\nabla(\gamma(\mathbf{v}))$ [5].

The unstable stacking fault energy (γ_{usf}) and intrinsic stacking fault energy (γ_{isf}), which represent energy barrier and local minimum of the γ surface, respectively, are useful in analyzing the nucleation of dislocations at the crack tip [7], the resistance of dislocations to glide [8], the dissociation of dislocations to partial ones [9], and the brittle/ductile behavior of materials [10]. According to Rice's analysis [7], the ductility and brittleness of materials can be understood as the competition between the dislocation emission from a crack tip and the crack cleavage, which can be described by the ductility parameter D, where D is proportional to free surface energy γ_s over unstable stacking faulty energy γ_{usf}. For example, the materials under pure mode I loading will be ductile if the ductility parameter $D = \frac{\gamma_s}{\gamma_{usf}}$ is bigger than 9.1 for FCC structures and 6.3 for BCC structures [7]. On the other hand, the relative value of the unstable stacking fault energy and unstable twinning fault energy has been used to identify the favored plastic deformation mechanism of metals [11], i.e. dislocation-slip-mediated or twinning-mediated plastic deformation.

In spite of the importance of GSFEs, measuring the SFE experimentally is not simple, i.e. indirectly from transmission electron microscopy (TEM) observations [12]. Such an experimental procedure is also time consuming and unable to obtain unstable stacking fault energies. Fortunately, theoretical studies on GSFEs become feasible and reliable, especially with the rapid increase in computing power, the progress in methodology and the development of efficient computational tools. Both embedded atom method (EAM) and DFT have been

* Corresponding authors.
E-mail addresses: xqzeng@sjtu.edu.cn (X. Zeng), hong.zhu@sjtu.edu.cn (H. Zhu).

https://doi.org/10.1016/j.commatsci.2018.12.013
Received 14 September 2018; Received in revised form 4 December 2018; Accepted 5 December 2018

used to study GSFEs. For example, γ surface of Mg [9,13], Ti [14], Zr [17,18], Fe [16], Ni, Cu and Al [17] based on EAM or MEAM (Modified EAM) usually tend to underestimate the energy barrier as compared to first principles calculations [9,16–18]. Besides, EAM would sometimes produce spurious metastable states along the GSFE surface of {0 0 0 1} or {1 0 $\bar{1}$ 0} plane [13,15] in HCP structures, which were determined to be not stable or would dissociate based on ab initio calculations. Compared with the methods of semi-empirical potentials, the GSFEs can be calculated more accurately using first principles calculations, which are becoming prevailing in studying GSFEs. For example, by conducting first principles calculations on Al, Cu, Pt and other FCC metals, Wang et al. [19] found that their dislocations on {1 1 1} planes will dissociate, and explained the deformation mechanism in terms of the $\gamma_{usf}/\gamma_{isf}$ ratio. On the other hand, Yin and Wu [20] analyzed and studied comprehensively about the GSFEs on 5 slip planes for 6 HCP metals based on first principle calculations. Poty et al. [21] also focused on the HCP structures and found that the slipping along the ⟨1 1 $\bar{2}$ 0⟩ direction on the {1 0 $\bar{1}$ 0} plane is the easiest one for Ti and Zr.

In spite of these rapid progresses, the determinations of GSFEs based on first principles calculations usually require the understanding about the slip plane and Burgers vector for different crystal structures, the generation of perfect and faulted slab models with the proper surface orientation from bulk unit cells, and the GSFE calculations e.g. based on nudged elastic band (NEB) simulations. The success of such complex GSFE calculations relies heavily on the human intuition and manual operations on the atomic model building, simulation parameter adjustments, and final result analyses. These difficulties can lead to inefficiency and have been obstacles for large-scale investigations of material properties including GSFE. In fact, there are many efforts on high-throughput computation frameworks in recent years to speed up materials design, by solving the computational execution details and automating tasks, which are used to being performed manually. Such efforts could be found in diverse workflow managers and materials analysis libraries, including atomate [22], pymatgen [23], AFLOW [24], AiiDA [25], MAST [26], OQMD [27], ASE [28] and ioChem-BD [29].

In this paper, we present a high-throughput computational framework to determine the generalized stacking fault energies based on density functional theory (DFT) simulations. Firstly, we present the algorithms and workflows for GSFE determinations of pure metals along typical slip planes and slip directions using the infrastructures of the Materials Project [30]. To validate our method, we have determined the GSFE profiles for 11 metals along possible slip planes, which were compared with available literature data and analyzed in terms of the preferred slip system, the tendency for dislocation dissociations, and the ductility of the materials.

2. Computational methods

2.1. DFT calculations

The GSFEs can be obtained by incrementally shifting the upper half crystal along the slip direction by a vector $\boldsymbol{\nu}$ and calculating the energy difference per unit area between the faulted slab and the perfect slab:

$$\gamma(\nu) = \frac{E(\boldsymbol{\nu}) - E_0}{A} \quad (1)$$

$E(\boldsymbol{\nu})$ is the total energy of the faulted slab, the top part of which shifted with respect to the bottom by a vector $\boldsymbol{\nu}$, E_0 stands for the energy of the perfect slab, A represents the area of the fault plane, and the stacking fault vector $\boldsymbol{\nu}$ varies from 0.0**b** to 1.0**b** (**b** is the Burgers vector). We used the climbing image-nudged elastic band (CI-NEB) method [31] to determine the γ curves of crystal slips with precise values of saddle points γ_{usf}, because the accuracy of conventional GSFE calculation based on first principles by only relaxing atoms in perpendicular direction to slip planes could be improved by conducting NEB calculations [32]. In an NEB calculation, two endpoint structures and several intermediate structures are needed. In order to achieve the force and energy convergence criteria, global force NEB optimizations (instead of image by image) were performed by using image dependent pair potential (IDPP) algorithm [33]. The relaxation of ions was stopped when the force convergence of 10 and 30 meV/Å for endpoint structure relaxations and NEB image structure calculations are achieved, respectively. At the same time, energy convergences of 0.1 meV were reached for each slab model. The total energy calculations in this work are performed in Vienna Ab Initio Simulation Package (VASP) [34,35] based on DFT, in which the Perdew-Burke-Ernzerhof (PBE) generalized gradient approximation (GGA) [36] and projector augmented wave (PAW) [37] pseudopotentials were used. The energy cut-off for the plane wave expansions is 520 eV and k-point mesh is generated automatically by pymatgen [23] with grid density of 2100 per reciprocal atom (pra), which means that the number of atoms per cell multiplied by the number of k-points equals approximately 2100. A large number of preliminary calculations were performed to establish the influence of slab thickness and vacuum thickness on the GSFE values, and finally, 12 atomic layer models with 15 Å vacuum were used.

2.2. Slip systems for GSFEs

After studying the crystallographic structures of pure metals in first five periods of the periodic table, we found that most pure metals adopt FCC, BCC and HCP crystal structures. Thus, we were especially interested in the slip systems of these three crystal structures, as shown in Fig. 1. For FCC metals, typical slip systems are $\frac{1}{2}\langle 0\ 1\ 1\rangle\{1\ 0\ 0\}$ and $\frac{1}{2}\langle 1\ 1\ 0\rangle\{1\ 1\ 1\}$, where the latter slip system consists of close packed planes {1 1 1} and close packed direction ⟨1 1 0⟩ of FCC structure. For BCC metals, the slip system of $\frac{1}{2}\langle 1\ 1\ 1\rangle\{1\ 1\ 0\}$ with the close packed planes and close packed direction was studied. As for HCP structures, the slip directions include ⟨1 1 $\bar{2}$ 0⟩ and ⟨1 1 $\bar{2}$ 3⟩, which are called ⟨a⟩ and ⟨a + c⟩ direction. In terms of slip planes, we can denote planes {0 0 0 1}, {1 0 $\bar{1}$ 0}, {1 0 $\bar{1}$ 1}, {1 1 $\bar{2}$ 2} as Basal, Prismatic, Pyramidal I and Pyramidal II respectively. Thus, the possible slip systems, $\frac{1}{3}\langle 1\ 1\ \bar{2}\ 0\rangle\{0\ 0\ 0\ 1\}$, $\frac{1}{3}\langle 1\ 1\ \bar{2}\ 0\rangle\{1\ 0\ \bar{1}\ 0\}$, $\frac{1}{3}\langle 1\ 1\ \bar{2}\ 0\rangle\{1\ 0\ \bar{1}\ 1\}$, $\frac{1}{3}\langle 1\ 1\ \bar{2}\ 3\rangle\{1\ 0\ \bar{1}\ 1\}$ and $\frac{1}{3}\langle 1\ 1\ \bar{2}\ 3\rangle\{1\ 1\ \bar{2}\ 2\}$, could be denoted by Basal ⟨a⟩, Prismatic ⟨a⟩, Pyramidal I ⟨a⟩, Pyramidal I ⟨a + c⟩ and Pyramidal II ⟨a + c⟩, respectively.

2.3. Workflow for GSFE calculations

The flowchart in Fig. 2 describes the workflow to calculate the GSFEs based on CI-NEB method, where the minimal energy path (MEP) along the slip direction is determined. Two endpoint slab structures representing the start and end of this slip process are denoted as ep0 and ep1, respectively. Ep0 represents the perfect slab and ep1 is the faulted slab with the top half of which shifted by a Burgers vector with respect to the bottom half. In order to get these two endpoint structures, the needed inputs include (a) a structure object, which is the crystal structure that can be directly obtained from Materials Project database via the Materials API [30,38] or specifically provided by users, (b) a slab configuration, which includes the number of atomic layers of the slab, the supercell size and doping condition of the slab, (c) VASP input settings, namely, the INCAR and KPOINTS settings, which can be generated from pymatgen [23] and pymatgen-diffusion [39], the latter package is the add-on to the former package for diffusion analysis that is developed by the Material Virtual Lab, and (d) slip systems of each crystal structure, which has been pre-defined for FCC, BCC and HCP crystal structures or could be also provided by users for other crystal structures.

After getting the crystal structure and user-specified configurations of slabs, the bulk crystal structure will be transformed into the slip-plane-oriented slab model, namely ep0 structure. Based on the

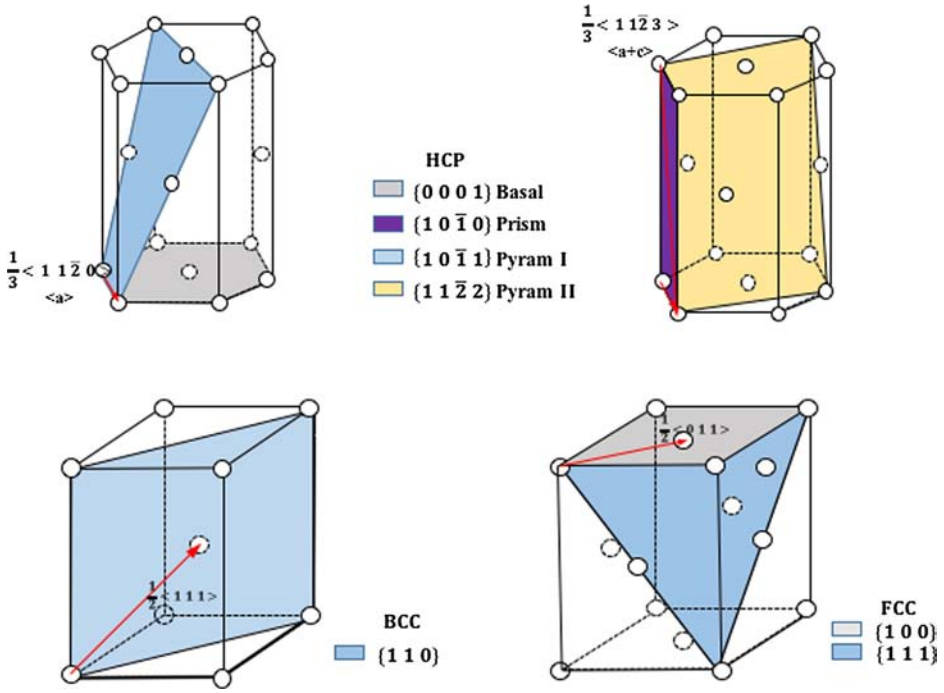

Fig. 1. Slip systems of HCP, BCC and FCC crystal structures. Slip planes are colored and denoted in the figure, while the slip directions are represented by red solid lines with arrows.

algorithm proposed by Sun et al. [40], a slab model with specific orientation could be generated from the bulk unit cell as the orange box in Fig. 2 shows. Firstly, the conventional unit cell is obtained from the bulk structure, after which, new basis vectors are constructed, two of which v_1 and v_2 constitute the slip plane, and another vector v_3 is the shortest Bravais lattice vector and as orthogonal to v_1 and v_2 as possible, a transformation matrix "slab_scale_factor" based on these new basis vectors is applied to transform a conventional unit cell into the reoriented conventional unit cell whose basal plane is the desired slip plane [40]. Then the large enough vacuum is introduced into the reoriented conventional unit cell to generate the slab model, and finally obtain a perfect primitive slab named ep0 and then the ep1 structure could be derived by slipping the top half of the ep0 slab with respect to the bottom part by a burger vector. After that, predeveloped automated fireworks for NEB calculations in atomate [22] will be used to relax two endpoint structures, and perform CI-NEB calculation along the path from ep0 to ep1. Here we generally used 8 images for HCP structures and 5 images for metals with FCC and BCC structures, which also could be specified by users. The output data of NEB workflow would be processed and stored into the MongoDb. The detailed description and code of workflow could refer to Supporting Information. All above operations are based on four Python software packages: atomate,

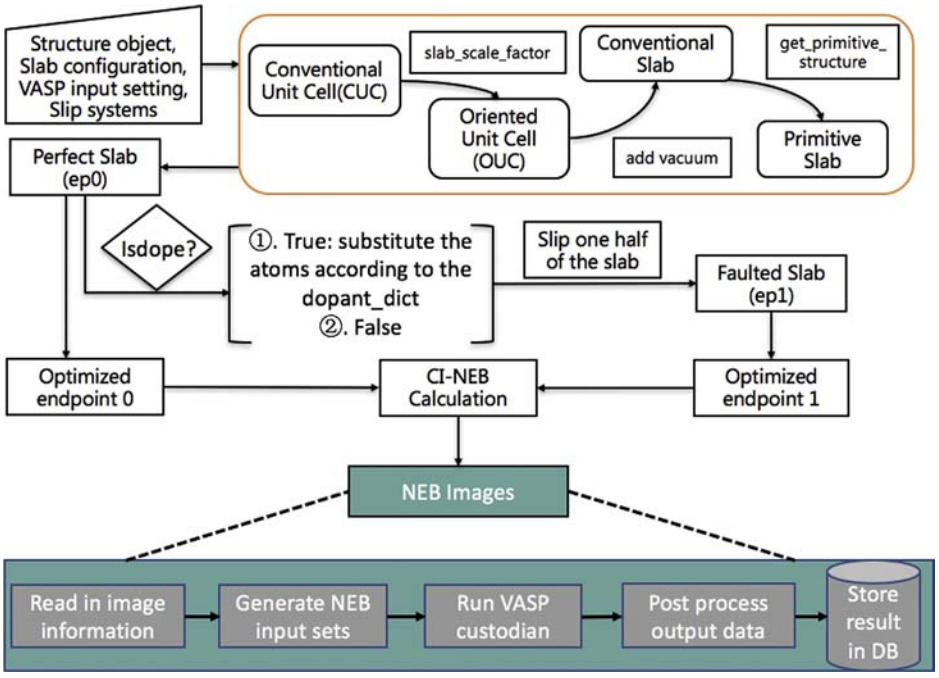

Fig. 2. Flowchart for GSFE Workflow based on DFT calculations.

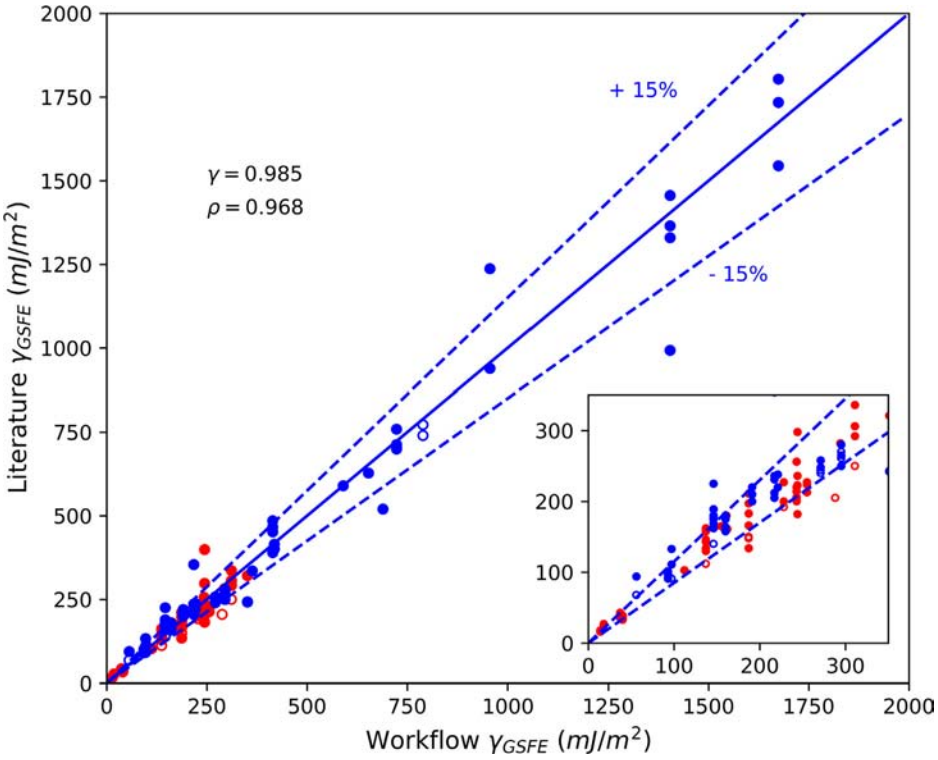

Fig. 3. Stacking fault energies from literatures versus those determined in this work, with Pearson and Spearman correlation coefficient (γ and ρ). Red and blue dots represent the intrinsic and unstable stacking fault energies γ_{isf} and γ_{usf}, respectively. The open circles represent GSFE obtained from literatures using NEB method while the solid circles represent data obtained from conventional static calculation method.

pymatgen, custodian [29] and fireworks [41]. The primary functions of pymatgen include building and transforming structures, generating input file and parsing output file. The fireworks library is for managing workflow and the atomate provides well-tested workflow templates to compute various materials properties such as electronic band structure, elastic properties, and piezoelectric, dielectric, and ferroelectric properties. And the errors come out during the calculation could be detected and fixed by custodian.

3. Results and discussions

3.1. Comparisons and validations

In order to validate our GSFE calculations based on CI-NEB method as well as the workflow algorithms, we compared the determined GSFEs in this work with those in literatures. Fig. 3 shows the stacking fault energy values in literatures versus those from this work, where the intrinsic and unstable stacking fault energies, namely γ_{isf} and γ_{usf}, are shown in red and blue, respectively. The stacking fault energies in literatures which are based on NEB method are shown in open circles, and those energies obtained by only relaxing atoms along the normal plane for a given atomic displacement along the slip plane are shown in solid circles. Dashed lines in Fig. 3 sets the boundary for the relative difference between this work and literatures of ± 15%, and the inset of the figure shows the stacking fault energies below 350 mJ/m^2. In general, our computational results have a good agreement with previous literature values, which can be also verified by the large Pearson and Spearman correlation coefficients (γ and ρ, respectively) of 0.985 and 0.968 respectively. However, we do observe the existence of some outliers in Fig. 3, which is due to the large variation of SFEs from different literatures. For example, the γ_{isf} of pyramidal II ⟨a + c⟩ in Mg is 244 mJ/m^2 in our work while the literature [9,20] values vary from 165 mJ/m^2 to 298 mJ/m^2, the difference with respect to our work is −32.4% and +22.1% respectively. And all values of stacking fault energy in these literatures are listed in the supplementary information Tables S1 and S2.

3.2. GSFEs for HCP metals

The HCP metals usually have poor formability or ductility compared to the FCC or BCC metals, because the activated slip systems for HCP metals at room temperature is much less than FCC and BCC owing to the low symmetry in HCP structures. Moreover, the interplanar distances between adjacent prismatic or pyramidal atomic planes of HCP structures could possess two different values [16,26] which could be denoted as W (wide) and N (narrow), respectively. The determined GSFEs for prismatic or pyramidal planes then will display two different curves, corresponding to deforming the top part of the slab with respect to the bottom at the large (W) and small (N) interplanar distance planes, respectively, this phenomenon could be called split slip mode. Thus, in total, there should be 8 types of slip modes in HCP structures considered in this work, including $\frac{1}{3}\langle 1\ 1\ \bar{2}\ 0\rangle\{0\ 0\ 0\ 1\}$ (Basal ⟨a⟩), $\frac{1}{3}\langle 1\ 1\ \bar{2}\ 0\rangle\{1\ 0\ \bar{1}\ 0\}$ with narrow and wide interplanar distance (Prism ⟨a⟩ N, Prism ⟨a⟩ W), $\frac{1}{3}\langle 1\ 1\ \bar{2}\ 0\rangle\{1\ 0\ \bar{1}\ 1\}$ with narrow and wide interplanar distance (Pyram I ⟨a⟩ N, Pyram I ⟨a⟩ W), $\frac{1}{3}\langle 1\ 1\ \bar{2}\ 3\rangle\{1\ 0\ \bar{1}\ 1\}$ with narrow and wide interplanar distance (Pyram I ⟨a + c⟩ N, Pyram I ⟨a + c⟩ W), and $\frac{1}{3}\langle 1\ 1\ \bar{2}\ 3\rangle\{1\ 1\ \bar{2}\ 2\}$ (Pyram II ⟨a + c⟩). However, slip modes having local minimum are very important in the sense of metallic plastic deformation, since it is related to the dislocation dissociations [9]. We focus our discussions on the five slip modes with local minimum of GSFE curves, which are shown in the Fig. 5: (a) Basal ⟨a⟩, (b) Prism ⟨a⟩ W, (c) Pyram I ⟨a⟩ N, (d) Pyram I ⟨a + c⟩ W and (e) Pyram II ⟨a + c⟩. On the prismatic plane with ⟨a⟩ direction and pyramidal I plane with ⟨a + c⟩ direction, the wide mode is energetically more favorable than the narrow mode because there exists a hollow site along the slip path of wide mode, and hence a local minimum in γ curve shown in Fig. 4. The similar situation also exists in pyramidal I plane with ⟨a⟩ direction, but conversely slipping on the narrow mode is more energetically favored, the detailed discussions could be found in supporting information.

Fig. 4 depicts the γ curves of Mg, Ti and Zr for the five slip modes which display local minima, and the γ_{isf} from literatures are also indicated with red circles and blue triangles, which represent the reported

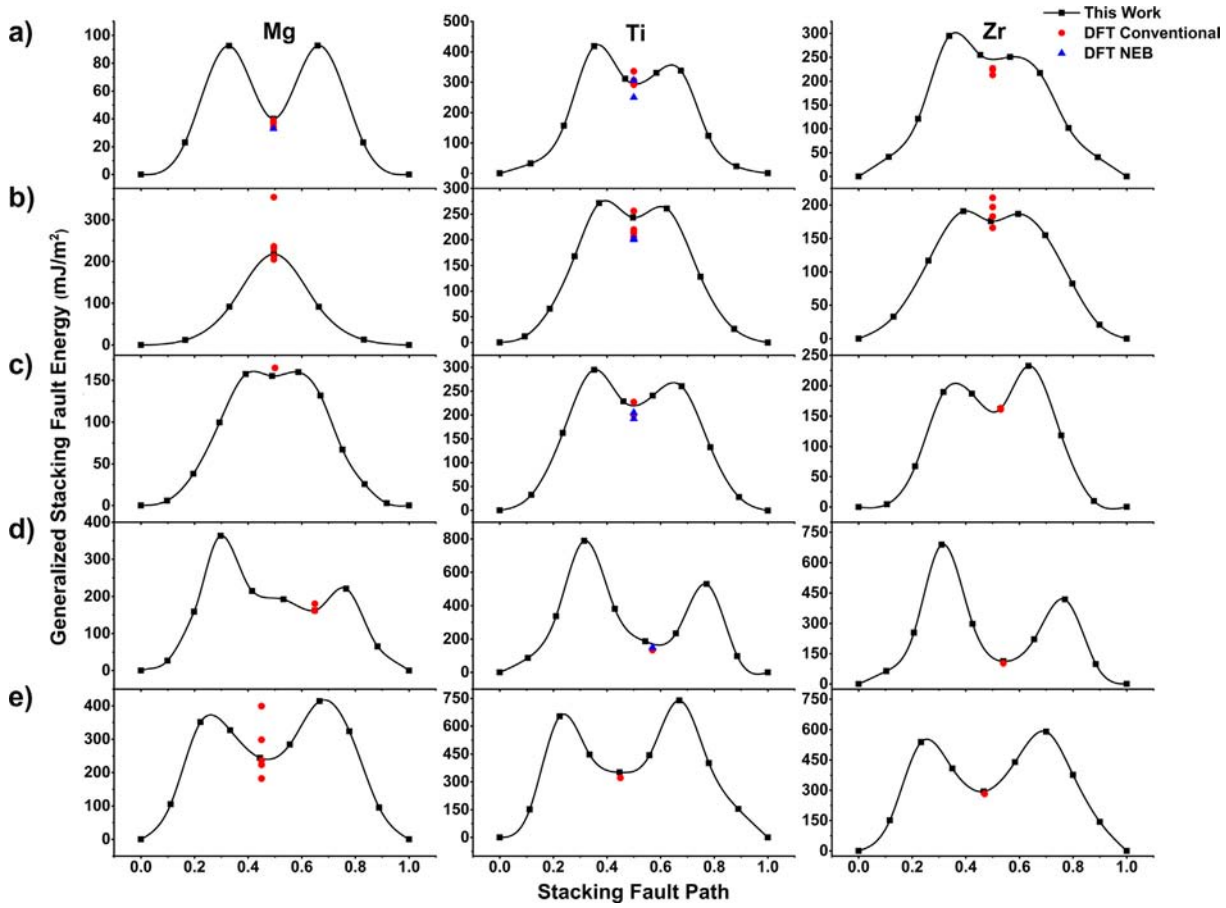

Fig. 4. GSFE curves of Mg, Ti and Zr in HCP structures for different slip systems: (a) $\frac{1}{3}\langle 1\ 1\ \bar{2}\ 0\rangle\{0\ 0\ 0\ 1\}$ (Basal ⟨a⟩), (b) $\frac{1}{3}\langle 1\ 1\ \bar{2}\ 0\rangle\{1\ 0\ \bar{1}\ 0\}$ with wide interplanar distance (Prism ⟨a⟩ W), (c) $\frac{1}{3}\langle 1\ 1\ \bar{2}\ 0\rangle\{1\ 0\ \bar{1}\ 1\}$ with narrow interplanar distance (Pyram I ⟨a⟩ N), (d) $\frac{1}{3}\langle 1\ 1\ \bar{2}\ 3\rangle\{1\ 0\ \bar{1}\ 1\}$ with wide interplanar distance (Pyram I ⟨a + c⟩ W), (e) $\frac{1}{3}\langle 1\ 1\ \bar{2}\ 3\rangle\{1\ 1\ \bar{2}\ 2\}$ (Pyram II ⟨a + c⟩). The data from literatures are also displayed, where the red circles are the literature data by only relaxing atoms along normal direction to slip plane in DFT calculations, and the blue triangles are the literature values obtained with NEB method.

γ_{isf} computed based on conventional static method and NEB method, respectively. All slip modes show a metastable stacking fault energy apart from the Prism ⟨a⟩ W mode of Mg. We can also note that these three HCP metals display similar GSFE curves for most of the slip modes, while GSFEs of Ti and Zr are especially close to each other due to their similarity of atomic and electronic structure. In terms of each slip mode, the γ_{usf} and γ_{isf} of Mg are always smaller than Ti and Zr and the lowest energy barrier lies in the Basal ⟨a⟩ for Mg and Prism ⟨a⟩ W for Ti and Zr, indicating the dominant slip mode for Mg and Ti or Zr is Basal ⟨a⟩ and Prism ⟨a⟩ W, respectively, which is consistent with results of experimental critical resolved shear stresses (CRSS) [42–44]. Moreover, for the same slip mode, we can note Zr has lower SFE values than Ti, indicating Zr is easier to slip than Ti.

3.3. GSFEs for FCC & BCC metals

We have also applied the GSFE high-throughput simulation workflows to calculate the GSFE curves for 4 metals with FCC crystal structures including Cu, Al, Ag and Au and 4 metals with BCC crystal structures including Mo, W, Ta and Fe. First, we calculated the γ curves of $\frac{1}{2}\langle 1\ 1\ 0\rangle\{1\ 1\ 1\}$ slip system for FCC metals, which are symmetric with an energy minimum of γ_{isf}, indicating that a full dislocation dissociates into a pair of Shockley partials, consistent with literatures [19,45–47]. The atoms won't slip straightly along $[\bar{1}\ 1\ 0]$ direction, but tend to dissociate into two partial dislocations, which could be represented by the reaction of $\frac{1}{2}[\bar{1}\ 1\ 0] = \frac{1}{6}[\bar{2}\ 1\ 1] + \frac{1}{6}[\bar{1}\ 2\ \bar{1}]$. Therefore, as shown in Fig. 5, we calculated the GSFE curve along $\frac{1}{6}\langle\bar{2}\ 1\ 1\rangle$ direction on {1 1 1} planes, which is half of the GSFE curve of the $\frac{1}{2}\langle 1\ 1\ 0\rangle\{1\ 1\ 1\}$ slip system. The maximum value of GSFEs, γ_{usf}, represents the lowest energy barrier for dislocation nucleation [48]. We also found that the slipping on {1 1 1} plane along $\langle\bar{2}\ 1\ 1\rangle$ has smaller γ_{usf} and smaller γ_{isf} compared to that on {1 1 0} plane along ⟨0 1 1⟩ direction, indicating that the former is most likely to be the dominant slipping mode for FCC metals. On the other hand, all BCC metals yield very similar GSFE curves for $\frac{1}{2}\langle 1\ 1\ 1\rangle\{1\ 1\ 0\}$ slip system, in which no local minima are found. Since the absence of local minimum along $\frac{1}{2}\langle 1\ 1\ 1\rangle$ direction on {1 1 0} of BCC, neither the metastable configuration nor the dislocation dissociation along the slip direction would be expected, which is generally accepted in bcc materials [16,49–51].

Among the four metals with FCC structures considered in this work, we can see the γ_{usf} along {1 1 1} plane is in the order of Cu > Al > Ag > Au, indicating Au is the metal easiest to slip. Similarly, for BCC structure Ta is the easiest one to slip among the four BCC metals considered here. Regardless of the importance of γ_{usf} and γ_{isf} on the analysis of materials' ductility, only relying on these two values is not enough. As mentioned before, the ratio of surface energy γ_s and unstable stacking fault energy γ_{usf} is a good criterion of metallic ductility [7]. If γ_s is small relative to γ_{usf} then the metal will tend to fail by cleavage fractures rather than shearing by dislocation-mediated slips. Here we list the D parameters of this work, Rice's work [7] and Mehl's work [52] for metals considered in this work in the Table 1, the surface energy data of this work are obtained from Tran et al. [53]. As we can see, for the four FCC metals, Al has the smallest D parameter while Au has the greatest D, and Cu has similar D parameter to Ag,

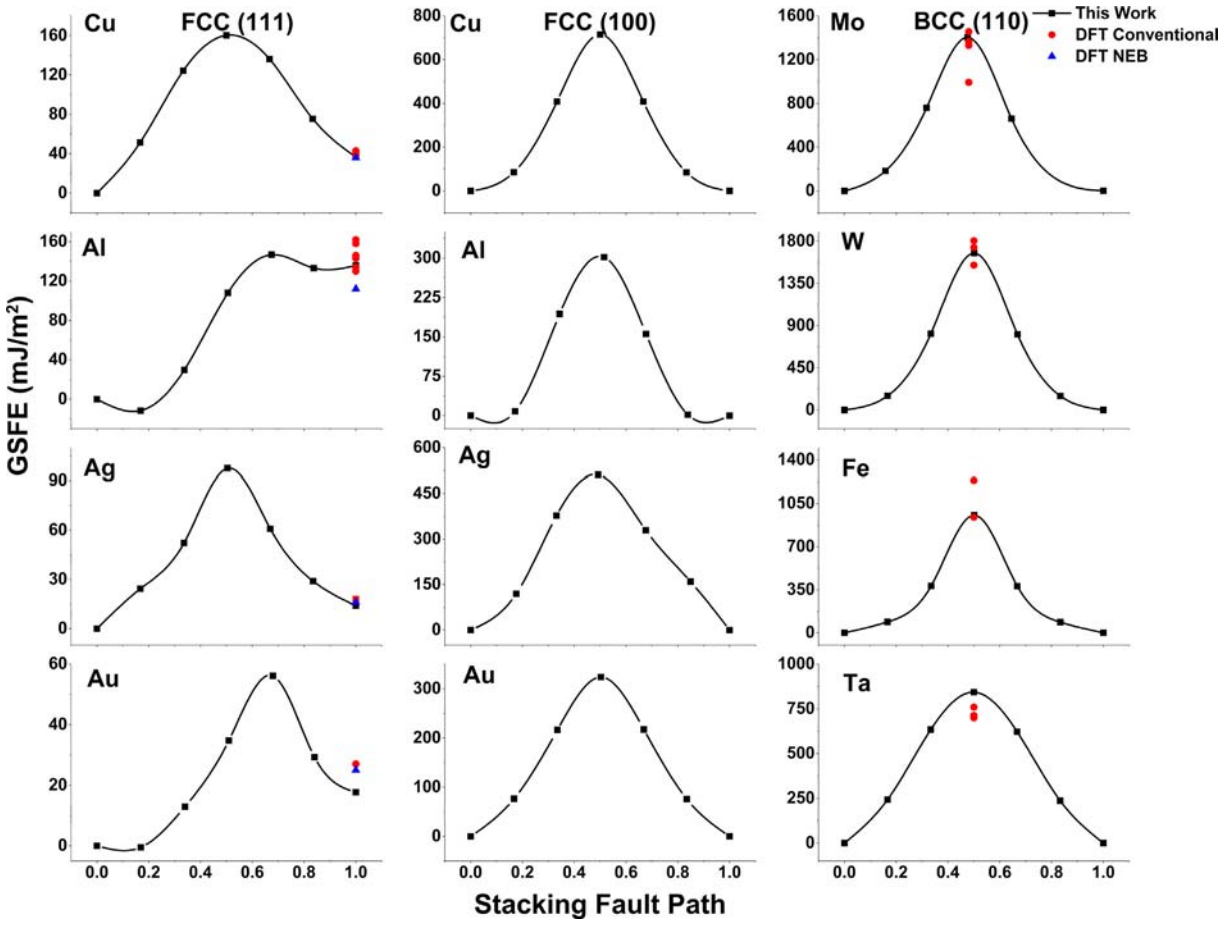

Fig. 5. GSFE curves of FCC metals including Cu, Al, Ag and Au in two slip systems, $\frac{1}{6}\langle\bar{2}\ 1\ 1\rangle\{1\ 1\ 1\}$ and $\frac{1}{2}\langle 0\ 1\ 1\rangle\{1\ 0\ 0\}$ and BCC metals including Mo, W, Ta and Fe for the $\frac{1}{2}\langle 1\ 1\ 1\rangle\{1\ 1\ 0\}$ slip system.

Table 1
Surface energy (γ_s), unstable stacking energy (γ_{usf}) and ductility parameters (D) for FCC and BCC metals, the slip plane for FCC is {1 1 1}, and for BCC is {1 0 0}, the D values from other literatures[7,52] are shown in parenthesis.

Element	γ_s (J/m^2)	γ_{usf} (J/m^2)	D (γ_s/γ_{usf})
FCC metals:			
Cu	1.31	0.160	8.188 (11.8[7], 10.68[52])
Al	0.80	0.146	5.479 (11.5[7], 4.94[52])
Ag	0.77	0.097	7.938 (12.5[7], 10.56[52])
Au	0.74	0.056	13.214 (15.7[7], 11.47[52])
BCC metals:			
Ta	2.34	0.723	3.237 (3.7[7])
Fe	2.45	0.956	2.563 (3.2[7])
W	3.23	1.674	1.930 (1.6[7])
Mo	2.80	1.404	1.994 (1.5[7])

which is also completely consistent with Mehl's result. Thus, we can note that Cu and Ag have similar ductility, and both of them are less ductile than Au but more ductile than Al. As for BCC metals, the ductility parameter D is generally small and there is no vast variance among the four metals considered. Relatively, Ta has better ductility than other three BCC metals. Generally speaking, the D parameters of FCC and BCC metals are relatively consistent with empirical ductility ranking. Moreover, both the results of ductility comparison in FCC and BCC are consistent with the Rice [7]'s in general, and the D parameters of FCC are always bigger than those of BCC, which conform to the idea that FCC metals always exhibit more ductility than BCC structures.

4. Conclusion

In summary, this paper presents a high-throughput framework to calculate the generalized stacking fault energies of pure metals based on DFT calculations and CI-NEB method. This framework realizes the automation of building the perfect and faulted slab for certain slip system, performing first principle NEB calculations and analyzing the GSFEs and storing into database. The results of stacking fault energy have a good agreement with the data from previous literatures. Different slip modes, γ curve and ductility of more than 10 metal elements have been discussed and demonstrated. This workflow may be used to predict GSFEs of amounts of other metals or alloys and accelerate the development and understanding of their mechanical properties.

5. Data availability

The raw/processed data required to reproduce these findings cannot be shared at this time due to time limitations.

Conflicts of interest

The authors declare no financial competing interests.

CRediT authorship contribution statement

Peng Tu: Conceptualization, Data curation, Formal analysis, Investigation, Methodology, Project administration, Software, Validation, Visualization, Writing - original draft, Writing - review & editing. **Yonghao Zheng:** Formal analysis, Investigation, Methodology, Validation. **Cheng Zhuang:** Formal analysis, Investigation, Methodology, Validation. **Xiaoqin Zeng:** Conceptualization, Funding acquisition, Resources, Supervision. **Hong Zhu:** Conceptualization, Formal analysis, Funding acquisition, Investigation, Methodology, Project administration, Resources, Supervision, Writing - original draft, Writing - review & editing.

Acknowledgement

The research was financially supported by the National Key Research and Development Program of China, China (No. 2017YFB0701500 and No. 2016YFB0701202) and the National Natural Science Foundation of China, China (General Program No. 51474149). First-principles calculations were carried out with computational resources from Shanghai Jiao Tong University Super Computer Center. H. Zhu also thanks to the financial support from the University of Michigan (U-M) and Shanghai Jiao Tong University (SJTU) joint funding, China (AE604401). The authors also would like to acknowledge work from Materials Project and Hacking Materials research group on the atomate and other packages used to implement the workflow outlined herein.

Appendix A. Supplementary material

Supplementary data to this article can be found online at https://doi.org/10.1016/j.commatsci.2018.12.013.

References

[1] G.I. Taylor, The mechanism of plastic deformation of crystals. Part II—Comparison with observations, Proc. R. Soc. London Ser. A 145 (1934) 388–404.
[2] F.R.N. Nabarro, Dislocations in a simple cubic lattice, Proc. Phys. Soc. 59 (1947) 256–272.
[3] R. Peierls, the size of a dislocation, Proc. Phys. Soc. 52 (1940).
[4] M.S. Duesbery, The influence of core structure on dislocation mobility, Philos. Mag. 19 (1969) 501–526.
[5] V. Vitek, Structure of dislocation cores in metallic materials and its impact on their plastic behaviour, Prog. Mater. Sci. 36 (1992) 1–27.
[6] V. Vítek, Intrinsic stacking faults in body-centred cubic crystals, Philos. Mag. 18 (1968) 773–786.
[7] J.R. Rice, Dislocation nucleation from a crack tip: an analysis based on the Peierls concept, J. Mech. Phys. Solids 40 (1992) 239–271.
[8] S.K. Yadav, X.Y. Liu, J. Wang, R. Ramprasad, A. Misra, R.G. Hoagland, First-principles density functional theory study of generalized stacking faults in TiN and MgO, Philos. Mag. 94 (2014) 464–475.
[9] Z. Pei, L.F. Zhu, M. Friák, S. Sandlöbes, J. Von Pezold, H.W. Sheng, C.P. Race, S. Zaefferer, B. Svendsen, D. Raabe, J. Neugebauer, Ab initio and atomistic study of generalized stacking fault energies in Mg and Mg-Y alloys, New J. Phys. 15 (2013).
[10] Z. Wu, B. Yin, W.A. Curtin, Energetics of dislocation transformations in hcp metals, Acta Mater. 119 (2016) 203–217.
[11] H. Van Swygenhoven, P.M. Derlet, A.G. Frøseth, Stacking fault energies and slip in nanocrystalline metals, Nat. Mater. 3 (2004) 399–403, https://doi.org/10.1038/nmat1136.
[12] P. Dumitraschkewitz, H. Clemens, S. Mayer, D. Holec, Impact of alloying on stacking fault energies in γ-TiAl, Appl. Sci. 7 (2017) 1193.
[13] I. Shin, E.A. Carter, Orbital-free density functional theory simulations of dislocations in magnesium, Model. Simul. Mater. Sci. Eng. 20 (2012).
[14] M. Ghazisaeidi, D.R. Trinkle, Core structure of a screw dislocation in Ti from density functional theory and classical potentials, Acta Mater. 60 (2012) 1287–1292.
[15] E. Clouet, Screw dislocation in zirconium: an ab initio study, Phys. Rev. B. 144104 (2012) 1–11.
[16] L. Ventelon, F. Willaime, Generalized stacking-faults and screw-dislocation core-structure in bcc iron: a comparison between ab initio calculations and empirical potentials, Philos. Mag. 90 (2010) 1063–1074.
[17] J.A. Zimmerman, H. Gao, F.F. Abraham, Generalized stacking fault energies for embedded atom FCC metals, Modell. Simul. Mater. Sci. Eng. 103 (2000).
[18] Q. Dong, Z. Luo, H. Zhu, L. Wang, T. Ying, Z. Jin, D. Li, W. Ding, X. Zeng, Basal-plane stacking-fault energies of Mg alloys: a first-principles study of metallic alloying effects, J. Mater. Sci. Technol. 34 (2018) 1773–1780.
[19] R. Wang, S. Wang, X. Wu, Edge dislocation core structures in FCC metals determined from ab initio calculations combined with the improved Peierls-Nabarro equation, Phys. Scr. 83 (2011).
[20] B. Yin, Z. Wu, W.A. Curtin, Comprehensive first-principles study of stable stacking faults in hcp metals, Acta Mater. 123 (2017) 223–234.
[21] A. Poty, J.M. Raulot, H. Xu, J. Bai, C. Schuman, J.S. Lecomte, M.J. Philippe, C. Esling, Classification of the critical resolved shear stress in the hexagonal-close-packed materials by atomic simulation: application to -zirconium and -titanium, J. Appl. Phys. 110 (2011).
[22] K. Mathew, J.H. Montoya, A. Faghaninia, S. Dwarakanath, M. Aykol, H. Tang, I. Heng Chu, T. Smidt, B. Bocklund, M. Horton, J. Dagdelen, B. Wood, Z.K. Liu, J. Neaton, S.P. Ong, K. Persson, A. Jain, Atomate: a high-level interface to generate, execute, and analyze computational materials science workflows, Comput. Mater. Sci. 139 (2017) 140–152.
[23] S.P. Ong, W.D. Richards, A. Jain, G. Hautier, M. Kocher, S. Cholia, D. Gunter, V.L. Chevrier, K.A. Persson, G. Ceder, Python materials genomics (pymatgen): a robust, open-source python library for materials analysis, Comput. Mater. Sci. 68 (2013) 314–319.
[24] S. Curtarolo, W. Setyawan, G.L.W. Hart, M. Jahnatek, R.V. Chepulskii, R.H. Taylor, S. Wang, J. Xue, K. Yang, O. Levy, M.J. Mehl, H.T. Stokes, D.O. Demchenko, D. Morgan, AFLOW: an automatic framework for high-throughput materials discovery, Comput. Mater. Sci. 58 (2012) 218–226.
[25] G. Pizzi, A. Cepellotti, R. Sabatini, N. Marzari, B. Kozinsky, AiiDA: automated interactive infrastructure and database for computational science, Comput. Mater. Sci. 111 (2016) 218–230.
[26] T. Mayeshiba, H. Wu, T. Angsten, A. Kaczmarowski, Z. Song, G. Jenness, W. Xie, D. Morgan, The MAterials Simulation Toolkit (MAST) for atomistic modeling of defects and diffusion, Comput. Mater. Sci. 126 (2017) 90–102.
[27] J.E. Saal, S. Kirklin, M. Aykol, B. Meredig, C. Wolverton, Materials design and discovery with high-throughput density functional theory: the open quantum materials database (OQMD), JOM 65 (2013) 1501–1509.
[28] S.R. Bahn, K.W. Jacobsen, An object-oriented scripting interface to a legacy electronic structure code, Comput. Sci. Eng. 4 (2002) 56–66.
[29] C. De Graaf, N. Lo, F. Maseras, J.M. Poblet, C. Bo, Managing the computational chemistry big data problem: the ioChem-BD platform, J. Chem. Inform. Model. (2015).
[30] A. Jain, S.P. Ong, G. Hautier, W. Chen, W.D. Richards, S. Dacek, S. Cholia, D. Gunter, D. Skinner, G. Ceder, K.A. Persson, Commentary: The materials project: a materials genome approach to accelerating materials innovation, APL Mater. 1 (2013).
[31] G. Henkelman, B.P. Uberuaga, H. Jónsson, Climbing image nudged elastic band method for finding saddle points and minimum energy paths, J. Chem. Phys. 113 (2000) 9901–9904.
[32] P. Kwaśniak, P. Śpiewak, H. Garbacz, K.J. Kurzydłowski, Plasticity of hexagonal systems: split slip modes and inverse Peierls relation in α-Ti, Phys. Rev. B - Condens. Matter Mater. Phys. 89 (2014) 1–6.
[33] S. Smidstrup, A. Pedersen, K. Stokbro, H. Jónsson, Improved initial guess for minimum energy path calculations, J. Chem. Phys. 140 (2014).
[34] G. Kresse, J. Furthmüller, Efficient iterative schemes for ab initio total-energy calculations using a plane-wave basis set, Phys. Rev. B - Condens. Matter Mater. Phys. 54 (1996) 11169–11186.
[35] G. Kresse, J. Furthmüller, Efficiency of ab-initio total energy calculations for metals and semiconductors using a plane-wave basis set, Comput. Mater. Sci. 6 (1996) 15–50.
[36] J.P. Perdew, K. Burke, M. Ernzerhof, Generalized gradient approximation made simple, Phys. Rev. Lett. 77 (1996) 3865–3868.
[37] P.E. Blöchl, Projector augmented-wave method, Phys. Rev. B 50 (1994) 17953–17979.
[38] S.P. Ong, S. Cholia, A. Jain, M. Brafman, D. Gunter, G. Ceder, K.A. Persson, The Materials Application Programming Interface (API): a simple, flexible and efficient API for materials data based on REpresentational State Transfer (REST) principles, Comput. Mater. Sci. 97 (2015) 209–215.
[39] Z. Deng, Z. Zhu, I.H. Chu, S.P. Ong, Data-driven first-principles methods for the study and design of alkali superionic conductors, Chem. Mater. 29 (2017) 281–288.
[40] W. Sun, G. Ceder, Efficient creation and convergence of surface slabs, Surf. Sci. 617 (2013) 53–59.
[41] L. Adhianto, S. Banerjee, M. Fagan, M. Krentel, G. Marin, J. Mellor-Crummey, N.R. Tallent, Fireworks: a dynamic workflow system designed for high- throughput applications, Concurr. Comput. Pract. Exp. 22 (2015) 685–701.
[42] S. Sandlobes, S. Zaefferer, I. Schestakow, S. Yi, R. Gonzalez-Martinez, On the role of non-basal deformation mechanisms for the ductility of Mg and Mg-Y alloys, Acta Mater. 59 (2011) 429–439.
[43] J. Gong, A.J. Wilkinson, Anisotropy in the plastic flow properties of single-crystal α titanium determined from micro-cantilever beams, Acta Mater. 57 (2009) 5693–5705.
[44] J. Gong, T. Benjamin Britton, M.A. Cuddihy, F.P.E. Dunne, A.J. Wilkinson, (a) Prismatic, (a) basal, and (c + a) slip strengths of commercially pure Zr by micro-cantilever tests, Acta Mater. 96 (2015) 249–257.
[45] M. Jahnátek, J. Hafner, M. Kraj, Shear deformation, ideal strength, and stacking fault formation of fcc metals: a density-functional study of Al and Cu, Phys. Rev. B. (2009).
[46] X.-Z. Wu, R. Wang, S.-F. Wang, Q.-Y. Wei, Ab initio calculations of generalized-stacking-fault energy surfaces and surface energies for FCC metals, Appl. Surf. Sci. 256 (2010) 6345–6349.
[47] S. Kibey, J.B. Liu, M.J. Curtis, D.D. Johnson, H. Sehitoglu, Effect of nitrogen on generalized stacking fault energy and stacking fault widths in high nitrogen steels,

Acta Mater. 54 (2006) 2991–3001.
[48] Y. Sun, E. Kaxiras, Slip energy barriers in aluminium and implications for ductile-brittle behaviour, Philos. Mag. A Phys. Condens. Matter, Struct. Defects Mech. Prop. 75 (1997) 1117–1127.
[49] J. Yan, C. Wang, S. Wang, Generalized-stacking-fault energy and dislocation properties in bcc Fe, Phys. Rev. B 174105 (2004) 1–5.
[50] L.H. Yang, M. Tang, J.A. Moriarty, Dislocations and plasticity in bcc transition metals at high pressure, Dislocat. Solids 16 (2009).
[51] S.L. Frederiksen, K.W. Jacobsen, Density functional theory studies of screw dislocation core structures in bcc metals, Philos. Mag. 83 (2003) 365–375.
[52] M.J. Mehl, D.A. Papaconstantopoulos, N. Kioussis, M. Herbranson, Tight-binding study of stacking fault energies and the Rice criterion of ductility in the fcc metals, Phys. Rev. B - Condens. Matter Mater. Phys. 61 (2000) 4894–4897.
[53] R. Tran, Z. Xu, B. Radhakrishnan, D. Winston, W. Sun, K.A. Persson, S.P. Ong, Data descriptor: surface energies of elemental crystals, Sci. Data 23 (2016) 1–13.